Solid-State Electronics 194 (2022) 108373

Contents lists available at ScienceDirect

Solid State Electronics

journal homepage: www.elsevier.com/locate/sse

# Interface effects in ultra-scaled MRAM cells

M. Bendra [a,b,*], S. Fiorentini [a,b], W. Goes [c], S. Selberherr [b], V. Sverdlov [a,b]

[a] Christian Doppler Laboratory for Nonvolatile Magnetoresistive Memory and Logic, TU Wien, Gußhausstraße 27-29, A-1040 Wien, Austria
[b] Institute for Microelectronics, TU Wien, Gußhausstraße 27-29, A-1040 Wien, Austria
[c] Silvaco Europe Ltd., Cambridge, United Kingdom

ARTICLE INFO

*Keywords:*
Spin-transfer torques
Ultra-scaled MRAM
Interfacial-perpendicular magnetic anisotropy

ABSTRACT

The development of advanced magnetic tunnel junctions with a single-digit nanometer footprint can be achieved using an elongated multilayered ferromagnetic free layer structure. We demonstrate the switching of a composite free layer consisting of two ferromagnets separated by an MgO layer and an additional capping MgO layer to boost perpendicular anisotropy. A proper design of the free layer and its interface-induced perpendicular anisotropy helps to achieve reliable switching.

## 1. Introduction

Emerging nonvolatile spin-transfer torque (STT) magnetoresistive random access memory (MRAM) is one of the most promising candidates for future memory due to excellent performance and CMOS compatibility for embedded applications [1]. STT-MRAM has been increasingly adopted as a reliable, persistent nonvolatile memory capable of supporting the growing computing memory demands from data centers to wearables, artificial intelligence [2], and IoT [3]. To replace the ubiquitous DRAM, scaling STT-MRAM down to achieve higher densities is a key task, as well as improving the endurance and write speed. STT-MRAM shows promise as universal memory, with the attributes of SRAM, DRAM, and small to medium capacity storage memory [4].

The design of advanced single-digit nanometer footprint MRAM cells requires precise knowledge of spin currents and torques in magnetic tunnel junctions (MTJs) with elongated free and reference layers. Interface induced effects, like the perpendicular anisotropy and the spin-transfer torque, must be carefully evaluated. For this purpose, we have successfully modeled the interface effects through the use of position-dependent parameters and applied them to a device with several tunnel barrier interfaces with a few nanometers diameter. The predicted switching behavior of ultra-scaled MRAM cells with several MgO interfaces agrees well with recent experiments [5].

A conventional MRAM cell consists of several layers, including a CoFeB reference layer (RL) and a free magnetic layer (FL) separated by an MgO tunnel barrier (TB) or by an nonmagnetic spacer (NMS), c.f. Fig. 1 (b) and (c). The magnetization configuration perpendicular to the TB is determined by the anisotropy induced by the interface at the CoFeB|MgO interface. To further increase the perpendicular magnetic anisotropy, additional CoFeB|MgO interfaces are added in the FL, c.f. Fig. 1 (a) [6]. To reduce the cell diameter and to further boost the perpendicular anisotropy, one elongates the FL along the direction normal to the CoFeB|MgO interfaces [5]. With the length of the FL increasing to the order of or even larger than the diameter of the FL, the shape anisotropy becomes an important contribution to the perpendicular anisotropy. However, the interface-induced anisotropy still plays a decisive role in defining the switching of elongated composite FLs made of several pieces separated by MgO barriers as it will be demonstrated below.

## 2. Method

To demonstrate this behavior, we model the interface-induced anisotropy as (*i*) an average constant contribution to the uniaxial bulk anisotropy (shown in Fig. 2 (a) with the red-dashed line) and as (*ii*) localized near the interface (blue solid line in Fig. 2 (a)). We also consider two different behaviors for the transverse spin dephasing length shown in Fig. 2 (b). The value of the spin dephasing length determines the characteristic distance over which the non-equilibrium spin accumulation due to the electric current running through the structure decays from its maximum value at the FL interface to zero inside the FL. Therefore, the spin dephasing length defines the size of the layer close to the FL interface where the STT is acting. A short value of the dephasing length of $\lambda_\varphi = 0.4$ nm, near the interface (dot-dashed line Fig. 2 (b)) is in agreement with values in MTJs [7] and ensures rapid absorption of the transverse spin components and localizes the torques at the interfaces.

* Corresponding author.
*E-mail address:* bendra@iue.tuwien.ac.at (M. Bendra).

https://doi.org/10.1016/j.sse.2022.108373
Received 30 March 2022; Received in revised form 23 April 2022; Accepted 26 April 2022
Available online 10 May 2022
0038-1101/© 2022 The Author(s). Published by Elsevier Ltd. This is an open access article under the CC BY license (http://creativecommons.org/licenses/by/4.0/).

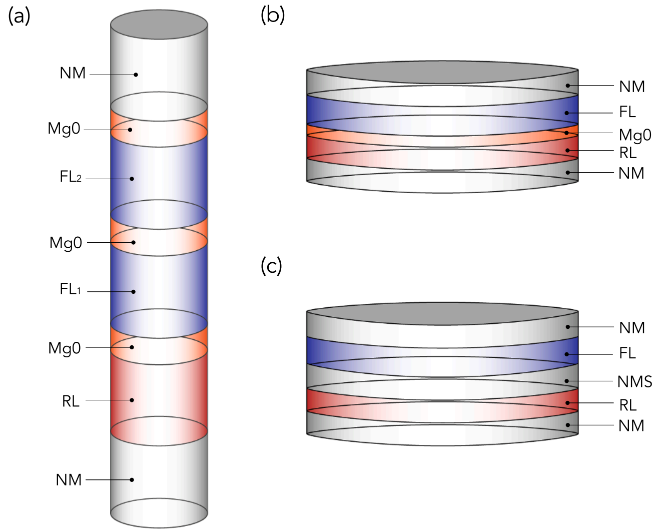


**Fig. 1.** Schematics: (a) Ultra-scaled MRAM cell with a diameter of 2.3 nm, made of a 5 nm RL, a 0.9 nm TB, and a composite FL, consisting of two ferromagnetic parts separated by a 0.9 nm MgO layer. The FL is capped by an additional MGO layer of 0.9 nm thickness. (b) Conventional MRAM cell with a diameter of 40 nm, made of a 1 nm RL, a 1.7 nm FL, and a 1 nm TB or (c) a NMS which consists of a 2 nm metal film.

In reality, the spin dephasing length increases away from the interfaces (blue line in Fig. 2 (b)), which allows the torques to act on larger portions of the FL. To model the dynamic properties of an ultra-scaled MRAM cell, we employ a fully three-dimensional finite element method including all physical phenomena, described with Eqs. (1)–(6). The magnetization dynamics are captured by the Landau-Lifshitz-Gilbert equation (LLG).

$$\frac{\partial \mathbf{m}}{\partial t} = -\gamma \mathbf{m} \times \mathbf{H}_{\text{eff}} + \alpha \mathbf{m} \times \frac{\partial \mathbf{m}}{\partial t} + \frac{1}{M_S}\mathbf{T}_{\mathbf{S}} \quad (1)$$

$\mathbf{m} = \mathbf{M}/M_S$ is the position-dependent normalized magnetization, $M_S$ is the saturation magnetization, $\alpha$ is the Gilbert damping constant, $\gamma$ is the gyromagnetic ratio, and $\mu_0$ is the vacuum permeability. The effective field $\mathbf{H}_{\text{eff}}$ includes the magnetic anisotropy field, the exchange field, and the demagnetization field. The latter contribution to $\mathbf{H}_{\text{eff}}$ is evaluated only on the disconnected magnetic domains by using a hybrid approach combining the boundary element method and the finite element method [8]. To appropriately model the switching of ultra-scaled MRAM cells the following equation is used for the torque $\mathbf{T}_{\mathbf{S}}$:

$$\mathbf{T}_{\mathbf{S}} = -\frac{D_e}{\lambda_J^2}\mathbf{m} \times \mathbf{S} - \frac{D_e}{\lambda_\varphi^2}\mathbf{m} \times (\mathbf{m} \times \mathbf{S}) \quad (2)$$

The torque is generated by a non-equilibrium spin accumulation $\mathbf{S}$ acting on the magnetization via the exchange interaction. $\lambda_J$ is the exchange length, $\lambda_\varphi$ is the spin dephasing length, $D_e$ is the electron diffusion coefficient in the ferromagnetic layers. The coupled spin and charge drift–diffusion model, as defined by Eqs. (3)–(5) supplemented by the appropriate boundary conditions of the spin accumulation and electric and spin current densities continuous over the interfaces, accurately describes the charge and the spin transport through a nanometer sized magnetic valve [9].

$$D_e\left(\frac{\mathbf{S}}{\lambda_{sf}^2} + \frac{\mathbf{S} \times \mathbf{m}}{\lambda_J^2} + \frac{\mathbf{m} \times (\mathbf{S} \times \mathbf{m})}{\lambda_\varphi^2}\right) = -\nabla \cdot \mathbf{J}_{\mathbf{S}} \quad (3)$$

$$\mathbf{J}_{\mathbf{S}} = -\frac{\mu_B}{e}\beta_\sigma\left(\mathbf{J}_{\mathbf{C}} \otimes \mathbf{m} + \beta_D D_e \frac{e}{\mu_B}[(\nabla \mathbf{S})\mathbf{m}] \otimes \mathbf{m}\right) - D_e \nabla \mathbf{S} \quad (4)$$

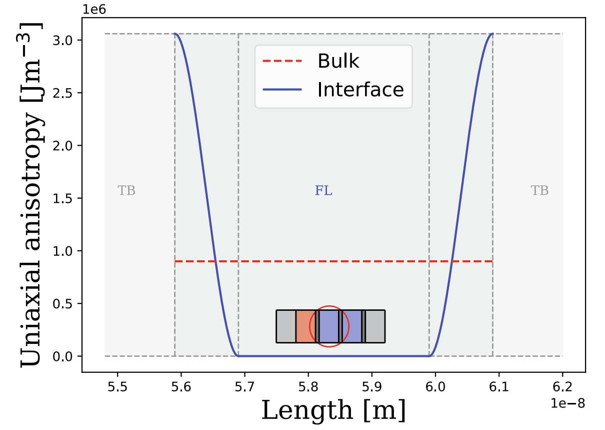


(a) The position-dependent development of interface anisotropy in blue, in comparison to a constant averaged anisotropy value applied within the 1st part of the FL red.

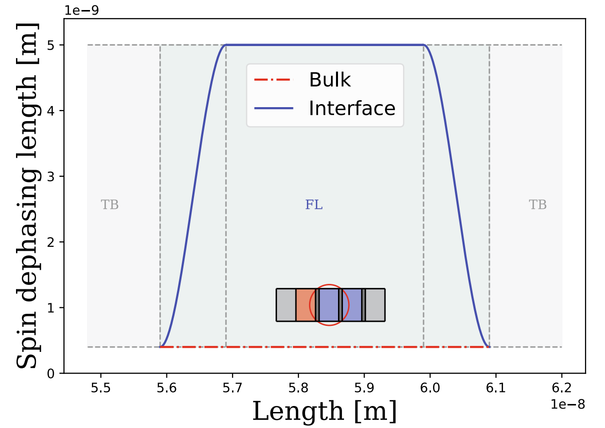


(b) The transverse spin dephasing length. The blue line represents the position-dependent development and the dashed red line the bulk/constant value, along the structure.

**Fig. 2.** Interface-induced perpendicular anisotropy and the transverse spin dephasing length.

$$\mathbf{J}_{\mathbf{C}} = \sigma \mathbf{E} - \beta_D D_e \frac{e}{\mu_B}[(\nabla \mathbf{S})\mathbf{m}] \quad (5)$$

$\mu_B$ is the Bohr magneton, $e$ is the electron charge, $\beta_\sigma$ and $\beta_D$ are polarization parameters. $\otimes$ is the outer product, $\mathbf{J}_{\mathbf{C}}$ is the charge current density, and $\mathbf{J}_{\mathbf{S}}$ is the spin current. We extended this method to MTJs by modeling the TB as a poor conductor with a local resistance (6) dependent on the relative orientation of the FL magnetization [10].

$$\sigma(\theta) = \frac{\sigma_P + \sigma_{AP}}{2}\left(1 + \left(\frac{\text{TMR}}{2 + \text{TMR}}\right)\cos\theta\right) \quad (6)$$

$\sigma_P$ ($\sigma_{AP}$) is the conductivity in the P (AP) state, and $\theta$ is the local angle between the magnetic vectors in the free and reference layer. TMR is the tunneling magnetoresistance ratio, defined as

$$\text{TMR} = \frac{G_P - G_{AP}}{G_{AP}} \quad (7)$$

where $G_P$ ($G_{AP}$) is the conductance in the P (AP) state. A high TMR is important to be able to read the conductance difference between the two configurations. When the electrons cross the RL, they become spin-polarized, generating a spin current. They then enter the FL, where

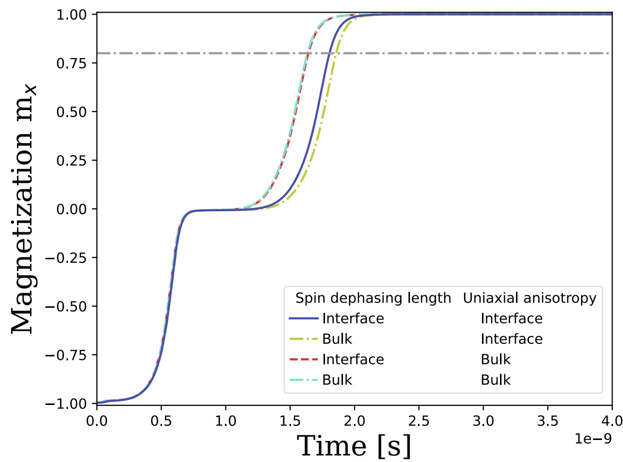


(a)

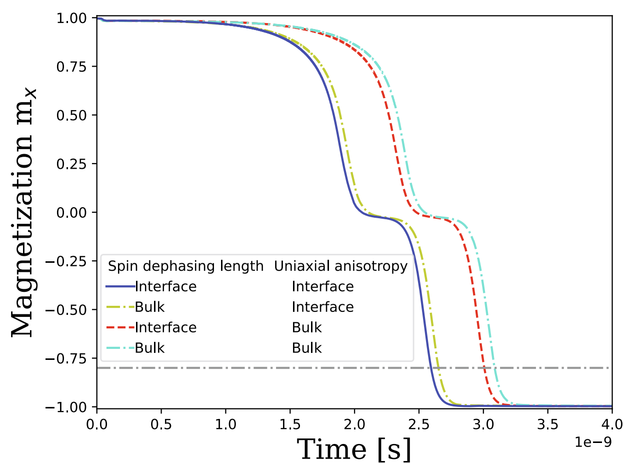


(b)

**Fig. 3.** Magnetization trajectories for switching from AP to P (a) and for P to AP (b), for various combinations of bulk and localized anisotropy and spin dephasing length. The horizontal gray dot-dashed line correspond to 80% switched.

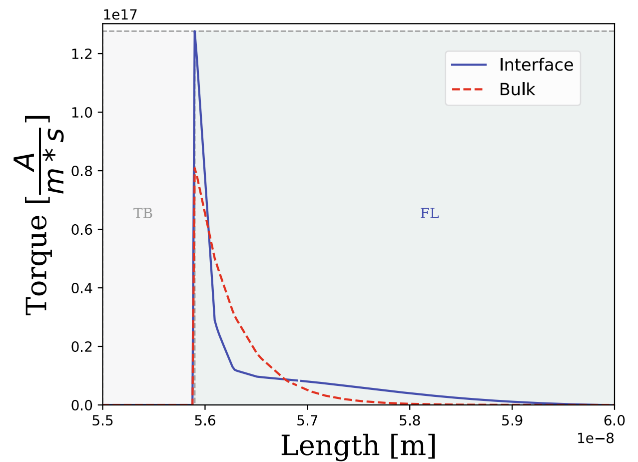


**Fig. 4.** Damping-like torques computed in a structure with semi-infinite ferromagnetic leads with a bias of $-2$ V and magnetization along $x$ in the RL and along z in the FL, for constant dephasing length in blue, and comparison to the position dependent dephasing length in red.

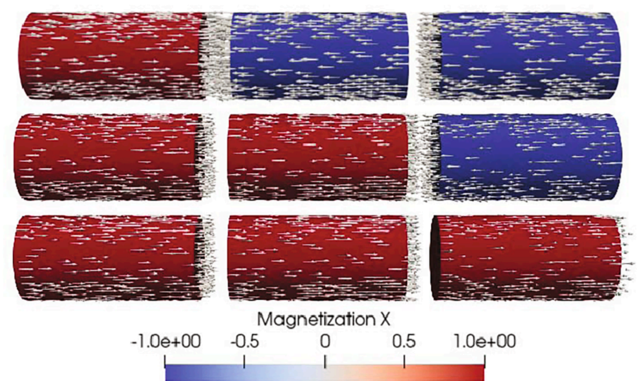


**(a)**

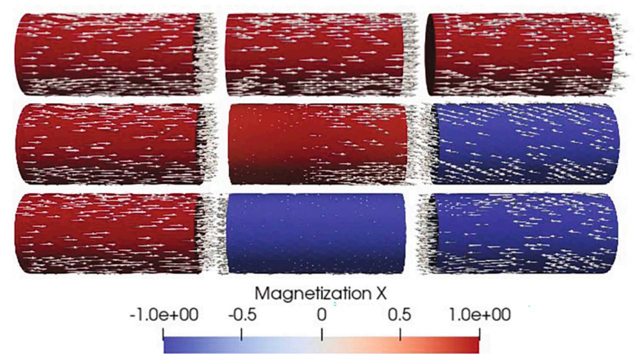


**(b)**

**Fig. 5.** Switching snapshot of MRAM cell's in the following order: Initial, intermediate and final state, for the configuration (a) AP to P and (b) P to AP. Arrows indicate the magnetization directions, and color-coding represents the average magnetization in $x$-direction.

the spin current acts on the magnetization. If the current is sufficiently strong, the magnetization of the free layer can be switched between the two stable configurations, parallel or anti-parallel, relative to the RL.

## 3. Results

The behavior of the FL magnetization projection orthogonal to the TBs, when the voltage pulse is applied, is shown in Fig. 3. Fig. 3 (a) demonstrates, under a bias of $-2$ V, the switching from AP to P configuration. In order to integrate the LLG Eq. (1) numerically, a backward-Euler scheme with a time step of $0.1ps$ was used. We have checked that a two times finer stepping does reproduce the same switching behavior for all models considered. This step is crucial for the simulation of the domain wall motion since the transition of the magnetization between the domains must be resolved. Failure to do so may result in artificial locking of the domain wall on the computational grid.

When switching from AP to P configuration, the magnetization reversal is very similar regardless of the model used. This indicates that the role of the interface-induced anisotropy as well as the dimension of the layer close to the interface, where the torque is acting, are not critical, and the switching, defined as the point where the magnetization crosses the 0.8 level, happens at about 1.9 nanoseconds. Fig. 3 (b) shows, however, that switching from P to AP with the bias of 2 V is accelerated, when the perpendicular magnetic anisotropy is interface-induced. The

role of the dephasing length on the switching within the models considered is negligible. It is due to the fact that in both models the torque acts very close to the interface as shown in Fig. 4.

There is a distinct peculiarity on the switching curves for both AP to P and P to AP switching. Namely, the magnetization of the FL develops a plateau around $m_x = 0$. The plateau is due to the fact that the magnetization of the two similar parts composing the FL are anti-parallel to each other. It then follows that the magnetization reversal is a sequential process in which one part of the FL switches first followed by the magnetization reversal of the remaining part. Fig. 5 (a) demonstrates the switching sequence for the AP to P process. In the AP configuration, both the RL and the second part of the FL (FL2) exert a torque on the first section of the FL (FL1) in the same sense, making it switch first. As the torques from the RL and the FL2 are additive, the switching of the FL1 is fast (Fig. 3 (a)). At the same time, the torque acting from the FL1 towards the FL2 is of the opposite sense and therefore preserves the FL2 orientation. However, after the magnetization of the FL1 is inverted and becomes parallel to that of the RL, the torque acting on the FL2 from the FL1 changes its sign forcing the FL2 to switch. As the torque acts only from the FL1, the magnitude of the torque acting on the FL2 is smaller than that previously acting on the FL1. The weaker torque results in a slower switching of the FL2 (c.f. Fig. 3 (a)).

When going from P to AP, the opposite process happens. Snapshots of the important stages of the switching process for the P to AP configuration are shown in Fig. 5 (b). The torque acting from the FL2 on the FL1 is opposite to that from the RL, so that the FL2 switches first. As only the torque from FL1 is acting on the FL2, the switching time of the FL2 is relatively slow. After the FL2 has switched, the torque contributions from the FL2 and the RL act on the FL1 in the same sense, completing the switching fast. As the parts of the FL are elongated, the exchange interaction is not sufficient to ensure a uniform macrospin-like switching of the FL1 and FL2 parts. The torques are the strongest close to the interface, so it is beneficiary to have the uniaxial anisotropy localized close to the interface where it can be easier overcome by the torques, to accelerate the switching at least for the P to AP switching. The overall switching behavior agrees well with results reported in experiments [5].

## 4. Conclusion

We demonstrated a successful design approach to ultra-scaled STT-MRAM consisting of several elongated pieces of ferromagnets separated by multiple tunnel barriers. The interface-induced anisotropy and the position-dependence of the transverse spin dephasing length are taken into account. We showed the influence of these effects on the magnetization dynamics as well as their role in improving the switching behavior in ultra-scaled MRAM cells. The predictions from our simulation results agree well with recent experimental demonstrations of switching of ultra-scaled MRAM cells.

## Declaration of Competing Interest

The authors declare that they have no known competing financial interests or personal relationships that could have appeared to influence the work reported in this paper.

## Acknowledgment

The financial support by the Austrian Federal Ministry for Digital and Economic Affairs, the National Foundation for Research, Technology and Development, and the Christian Doppler Research Association is gratefully acknowledged. The authors acknowledge TU Wien Bibliothek for financial support through its Open Access Funding Program.

## References

[1] Ito T, Saito T, Taito Y, Sonoda K, Watanabe G, et al. A 20Mb Embedded STT-MRAM Array Achieving 72% Write Energy Reduction with Self-termination Write Schemes in 16nm FinFET Logic Process. In: Ito, editor. 2021 IEEE International Electron Devices Meeting (IEDM); 2021. pp. 2.2.1–2.2.4. https://doi.org/10.1109/IEDM19574.2021.9720523.

[2] Chiu Y-C, Yang C-S, Teng S-H, Huang H-Y, Chang F-C, et al. A 22nm 4Mb STT-MRAM Data-Encrypted Near-Memory Computation Macro with a 192GB/s Read-and-Decryption Bandwidth and 25.1-55.1TOPS/W 8b MAC for AI Operations, in: 2022 IEEE International Solid- State Circuits Conference (ISSCC), vol. 65; 2022. p. 178–180. https://doi.org/10.1109/ISSCC42614.2022.9731621.

[3] Sun JJ, DeHerrera M, Hughes B, Ikegawa S, Lee HK, et al. Commercialization of 1Gb Standalone Spin-Transfer Torque MRAM. IEEE International Memory Workshop (IMW) 2021;2021:1–4. https://doi.org/10.1109/IMW51353.2021.9439616.

[4] Ikegawa S, Mancoff FB, Janesky J, Aggarwal S. Magnetoresistive Random Access Memory: Present and Future. IEEE Trans Electron Devices 2020;67(4):1407–19. https://doi.org/10.1109/TED.2020.2965403.

[5] Jinnai B, Igarashi J, Watanabe K, Funatsu T, Sato H, et al. High-Performance Shape-Anisotropy Magnetic Tunnel Junctions down to 2.3 nm. In: Jinnai, editor. 2020 IEEE International Electron Devices Meeting (IEDM); 2020. pp. 24.6.1–24.6.4. https://doi.org/10.1109/IEDM13553.2020.9371972.

[6] Khanal P, Zhou B, Andrade M, Dang Y, Davydov A, et al. Perpendicular magnetic tunnel junctions with multi-interface free layer. Appl Phys Lett 2021;119(24): 242404. https://doi.org/10.1063/5.0066782.

[7] Camsari KY, Ganguly S, Datta D, Datta S. Physics-based factorization of magnetic tunnel junctions for modeling and circuit simulation. In: 2014 IEEE International Electron Devices Meeting; 2014. https://doi.org/10.1109/IEDM.2014.7047177. pp. 35.6.1–35.6.4.

[8] Ender J, Mohamedou M, Fiorentini S, Orio R, Selberherr S, Goes W, et al. Efficient Demagnetizing Field Calculation for Disconnected Complex Geometries in STT-MRAM Cells. International Conference on Simulation of Semiconductor Processes and Devices (SISPAD) 2020;2020:213–6. https://doi.org/10.23919/SISPAD49475.2020.9241662.

[9] Petitjean C, Luc D, Waintal X. Unified Drift-Diffusion Theory for Transverse Spin Currents in Spin Valves, Domain Walls, and Other Textured Magnets. Phys Rev Lett 2012;109:117204. https://doi.org/10.1103/PhysRevLett.109.117204.

[10] Fiorentini S, Ender J, Selberherr S, de Orio R, Goes W, Sverdlov V. Coupled spin and charge drift-diffusion approach applied to magnetic tunnel junctions. Solid-State Electron 2021;186:108103. https://doi.org/10.1016/j.sse.2021.108103.

**Mario Bendra** was born in Steyr, Austria, in 1993. He received his Bachelor degree in Mechanical Engineering from the University of Applied Sciences Upper Austria in 2017. After an exchange semester at the University of the Sunshine Coast, Australia, in 2018, he received the degree of Diplomingenieur in Mechanical Engineering from the University of Applied Sciences Upper Austria in 2019. Mario joined the Christian Doppler Laboratory on Nonvolatile Magnetoresistive Memory and Logic in October 2020, where he is working towards his doctoral degree. His primary focus is developing and implementing advanced computational approaches to simulate and optimize spin-transfer torque in magnetoresistive memories.